Pentaerythritol Triacrylate-co-Trimethylolpropane Nanocomposite Scaffolds as Osteogenic Components for Bone Tissue Engineering

by

Mollie Marie Smoak

Undergraduate honors thesis under the guidance of

Dr. Daniel J Hayes

Department of Biological & Agricultural Engineering

Submitted to the Honors College in partial fulfillment of the Upper Division Honors Program

May, 2016

Louisiana State University

Baton Rouge, LA

Dedication

I would like to dedicate this thesis to the LA-STEM Program and the department of Biological and Agricultural Engineering at Louisiana State University. Before college, I was never immersed in science. Through the support and guidance of the faculty in OSI and BAE, I grew as a scientist, a scholar, and a citizen. I believe that I am a better person now than when I started college 4 years ago. Because you all have believed in me, I will be the first in my family to pursue a PhD. This is an accomplishment that I never thought I would be able to achieve 4 years ago. Thank you.

ACKNOWLEDGEMENTS

I would like to thank my parents for always believing in me even when I did not. They support every new endeavor that I want to explore and give me the confidence to try new things. I would like to thank my research advisors, Dr. Daniel Hayes, for giving me a chance from day one. He has always pushed me to go farther than I thought I was capable. He is the reason that I fell in love with research and will be continuing science as a career. I would like to thanks the graduate staff of both the Hayes and Monroe lab, especially Amar Quereshi, Nick Poche, Anoosha Forghani, and Lisa Kriegh. I have come to each of you for help, and each of you have helped to shape me as a scientist. I would also like to thank me best friend, Katie Hogan. Katie has been with me since the very beginning. She has pushed me to do great things and to never give up when times are hard. Because of her, I am a better person. Lastly, I would like to thank my graduate mentor, Cong Walker. He has laid down a great foundation for me. He believed in me from day one, and has given me every opportunity to grow and succeed in research. He opened up so many doors for me and is the reason that I have come as far as I have.

Table of Contents

PREFACE

This thesis contains research done during my undergraduate years in the Hayes/Monroe lab. I have reported on a project that was relevant to my growth as a researcher and my passion for tissue engineering. This report tells of my growth as a scientist by showcasing my first research project. Through this early project, I learned the basic skills that I would continue to utilize throughout my undergraduate research

ABSTRACT

An aging population in the United States is driving a growing demand for orthopedic surgeries and improvement in the repair of critical sized bone defects. Bone tissue engineering approaches using polymer/ceramic composites have shown promise as effective biocompatible, absorbable, and osteoinductive materials. In addition, it is ease of handling and effective repair of irregular-sized bone defects has been a concern. *In situ*-polymerizing thiol-acrylate based copolymers synthesized via an amine-catalyzed Michael addition was studied for its potential to be used in bone defect repair. Pentaerythritol triacrylate-co-trimethylolpropane tris(3-mercaptopropionate) (PETA-co-TMPTMP) composites were studied alone as well as with the incorporation of hydroxyapatite (HA) for the potential to induce osteogenesis in human adipose-derived stem cells (hASCs). The physical and mechanical properties of these materials were evaluated followed by an in vitro evaluation of the biocompatibility and chemical stability. In addition, an *in vivo* study was conducted to further examine the material's osteogenic potential.

Chapter 1. Introduction

1.1 The Clinical Need for Alternative Methods of Osteogenic Repair

As of 2010, close to 5.3 million orthopedic surgeries were performed each year, and this number is expected to increase to 6.2 million by 2020. For the past several decades, the standard treatment for a segmental skeletal defect has been to implant allografts and autografts to accelerate the healing process along with fixation using metal screws (Pallua, N., et al., 2010). These bone grafts have substantial limitations. Allografts, which are taken from donors, are limited by high cost, require time consuming bone banking procedures, and have increased risk of rejection and disease transmission. Autogenous bone grafts, which are the patient's own tissue, are limited by the quantity of tissue that can be accessed, additional surgeries to harvest and repair tissue, and an increased risk of donor site morbidity (Smoak, et al., 2014). Furthermore, these techniques do not address the need for a clinically convenient and biodegradable method for the conformal repair of critical sized bone defects while providing mechanical support and the biological cues necessary to promote bone regrowth. Although artificial composite scaffolds have been studied extensively as alternatives for bone grafting and augmentation, they have yet to see wide clinical adoption (Chen, et al., 2014).

1.2 Current biomaterials used in hASCs bone tissue engineering strategies

1.2.1 Synthetic Materials for Bone Regrowth

Synthetic polymers are often favored over natural-derived polymers because they can be manufactured reproducibly in bulk and in highly purified forms. In addition, many synthetic polymers have been shown to be biocompatible for bio inert. Unlike naturally-derived polymers, synthetic polymers possess easily tunable characteristics such as mechanical strength, surface morphology, degradation, and density in addition to surface functionality. Polyester polymers such

as polycaprolactone (PCL) and poly(l-lactic acid) (PLLA) have been shown to support hASCs proliferation and differentiation; they are the most popular synthetic polymeric materials in bone tissue engineering.(Guven et al., 2011; Jeon et al., 2008; Lee et al., 2011; Levi et al., 2010; Wang et al., 2010a)

Normally anionic polymerization mechanisms proceed via a chain growth mechanism. The polymer described in this study is produced via an amine catalyzed thiol-acrylate mechanism. This reaction proceeds through a chain "process" with sequential chain transfer steps with each addition causing the polymerization to follow the rules and attributes of a step growth mechanism in terms of molecular weight and physical properties. The general reaction scheme below is described in Bounds et al.(Bounds et al.)

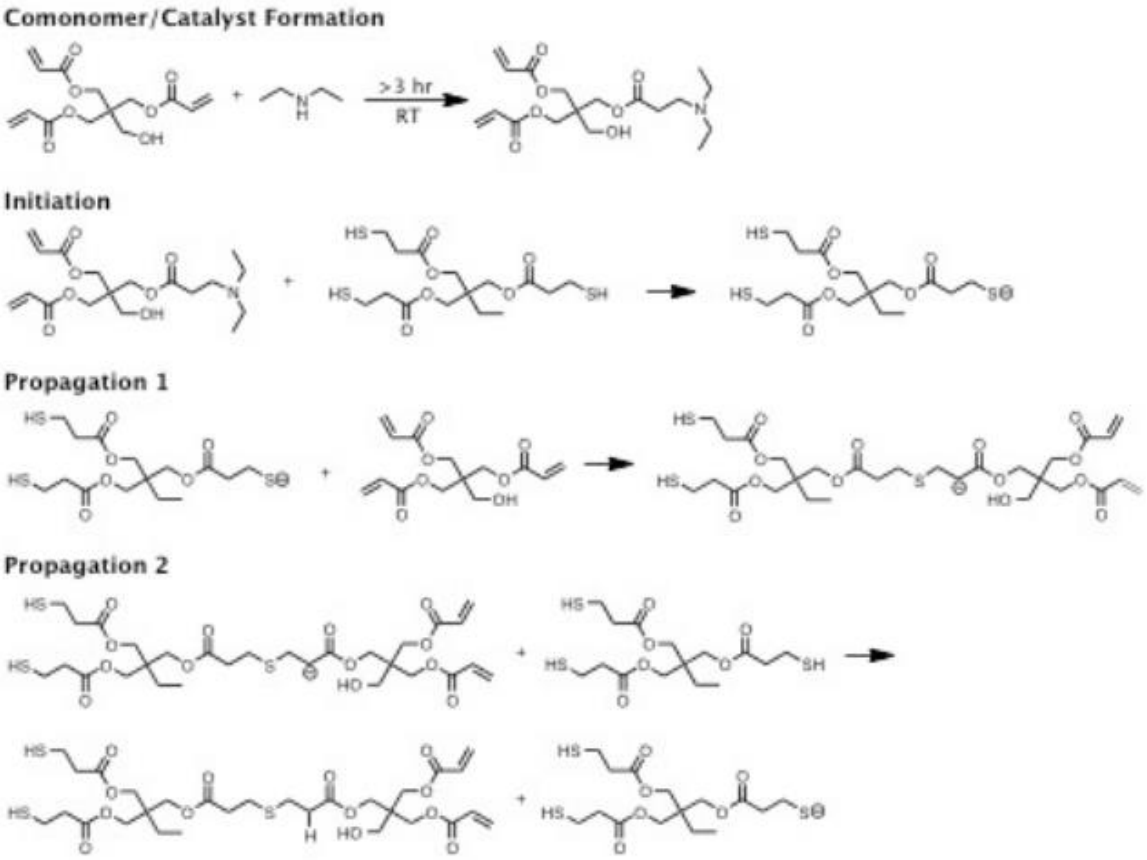

Figure 1.1 Scheme of Amine Catalyzed Thiol-Acrylate Reaction

1.2.2 Ceramics

Bone is composed of hydroxyapatite (HA) crystals distributed within an organic matrix with porosity and percent mineralization specific to individual bone types.(Pallua & Suscheck, 2010a) The use of calcium phosphate ceramics as bone substitutes dates back more than 30 years to the field of dental implantation (Ambard & Mueninghoff, 2006). However, one of the main disadvantage of calcium phosphates are their brittle nature and have poor fatigue resistance (Vallet-Regí & Ruiz-Hernández, 2011). While synthesis of highly porous bioceramics and scaffolds have shown increase cell migration as well as nutrient and waster transport, these materials have very poor mechanical properties. Consequently, for biomedical applications, calcium phosphates are primarily used as fillers and coatings.

1.3 Scaffolds fabrication method

1.3.1 Thermally induced phase separation

Bone scaffolds can be fabricated through the method of thermal precipitation to create a high volume of inter-connected micropores (Hutmacher, 2000). Briefly, the polymer was dissolved in organic solvents (1,4-dioxane or dimethylcarbonate) to produce a homogeneous mixture then mixed with ceramics powder. The solution was placed in a -70 °C freezer for 24 hours and lyophilized in a vacuum oven until a constant weight was attained (Maquet et al., 2004). These methods were utilized to prepare PCL/Hydroxyapatite control polymers (Zargarian & Haddadi-Asl, 2010)

1.3.2 Gas-Foaming Process

The process of gas foaming can also be used to fabricate polymer foams with high porosity without using toxic organic solvents (Cooper, 2000; Harris et al., 1998; Mooney et al., 1996). Carbon dioxide (CO2) is usually used as a gas porogen for foaming polymers. Solid polymers are saturated with CO2 when exposed to high pressure of CO2 gas. By using this approach, the porosity of polymer foam can reach up to 93% with pore size around 100 μm. However, gas-foaming results in a closed pore surface and with only 10–30% of interconnected pores.

1.4 Animal models used in bone tissue engineering

Rats are among of the most commonly used animals in medical research. However, there are significant dissimilarities between rat and human bones. Other animal models have been established to study parameters that affect bone healing. Rodents are inexpensive, easy to raise, and do not carry the societal concerns associated with using larger animal models (Liebschner, 2004). Multiple bone implants surgery models, such as spinal fusion, cranial defect and long

bone defect, have been used on rats and demonstrated great success (Burdick et al., 2003; Cook et al., 1994; Lopez et al., 2009). There are, however, disadvantages in the use of rats and mice: they have a limited naturally occurrence of basic multicellular unit based remodeling, and there is an absence of impaired osteoblast function during the late stages of estrogen deficiency (Liebschner, 2004). It is also impossible to collect large blood samples or obtain several biopsies in such a small animal for long term studies (Mooney & Siegel, 2005).

1.5 References

Ambard, A.J., Mueninghoff, L. 2006. Calcium Phosphate Cement: Review of Mechanical and Biological Properties. Journal of Prosthodontics, 15(5), 321-328.

Bounds, C.O., Goetter, R., Pojman, J.A., Vandersall, M. Preparation and application of microparticles prepared via the primary amine-catalyzed michael addition of a trithiol to a triacrylate. Journal of Polymer Science Part A: Polymer Chemistry, 50(3), 409-422.

Burdick, J.A., Frankel, D., Dernell, W.S., Anseth, K.S. 2003. An initial investigation of photocurable three-dimensional lactic acid based scaffolds in a critical-sized cranial defect. Biomaterials, 24(9), 1613-1620.

Cook, S.D., Baffes, G.C., Wolfe, M.W., SAMPATH, T.K., Rueger, D.C. 1994. Recombinant human bone morphogenetic protein-7 induces healing in a canine long-bone segmental defect model. Clinical orthopaedics and related research, 301, 302-312.

Cooper, A.I. 2000. Polymer synthesis and processing using supercritical carbon dioxide. Journal of Materials Chemistry, 10(2), 207-234.

Guven, S., Mehrkens, A., Saxer, F., Schaefer, D.J., Martinetti, R., Martin, I., Scherberich, A. 2011. Engineering of large osteogenic grafts with rapid engraftment capacity using mesenchymal and endothelial progenitors from human adipose tissue. Biomaterials, 32(25), 5801-9.

Harris, L.D., Kim, B.-S., Mooney, D.J. 1998. Open pore biodegradable matrices formed with gas foaming.

Hutmacher, D.W. 2000. Scaffolds in tissue engineering bone and cartilage. Biomaterials, 21(24), 2529-2543.

Jeon, O., Rhie, J.W., Kwon, I.K., Kim, J.H., Kim, B.S., Lee, S.H. 2008. In vivo bone formation following transplantation of human adipose-derived stromal cells that are not differentiated osteogenically. Tissue engineering. Part A, 14(8), 1285-94.

Lee, J.S., Lee, J.M., Im, G.I. 2011. Electroporation-mediated transfer of Runx2 and Osterix genes to enhance osteogenesis of adipose stem cells. Biomaterials, 32(3), 760-8.

Levi, B., James, A.W., Nelson, E.R., Vistnes, D., Wu, B., Lee, M., Gupta, A., Longaker, M.T. 2010. Human adipose derived stromal cells heal critical size mouse calvarial defects. PloS one, 5(6), e11177.

Liebschner, M.A. 2004. Biomechanical considerations of animal models used in tissue engineering of bone. Biomaterials, 25(9), 1697-1714.

Liebschner, M.A. 2004. Biomechanical considerations of animal models used in tissue engineering of bone. Biomaterials, 25(9), 1697-1714.

Lopez, M.J., McIntosh, K.R., Spencer, N.D., Borneman, J.N., Horswell, R., Anderson, P., Yu, G., Gaschen, L., Gimble, J.M. 2009. Acceleration of spinal fusion using syngeneic and allogeneic adult adipose derived stem cells in a rat model. Journal of Orthopaedic Research, 27(3), 366-373.

Maquet, V., Boccaccini, A.R., Pravata, L., Notingher, I., Jérôme, R. 2004. Porous poly (< i> α-hydroxyacid)/Bioglass< sup>® composite scaffolds for bone tissue engineering. I: preparation and in vitro characterisation. Biomaterials, 25(18), 4185-4194.

Mooney, D.J., Baldwin, D.F., Suh, N.P., Vacanti, J.P., Langer, R. 1996. Novel approach to fabricate porous sponges of poly (D, L-lactic-co-glycolic acid) without the use of organic solvents. Biomaterials, 17(14), 1417-1422.

Mooney, M.P., Siegel, M.I. 2005. Animal models for bone tissue engineering. Encyclopedia of Biomaterials and Biomedical Engineering. New York: Marcel Dekker, 1-19.

Pallua, N., Suscheck, C.V. 2010. Tissue engineering: from lab to clinic. Springer Verlag.

Vallet-Regí, M., Ruiz-Hernández, E. 2011. Bioceramics: from bone regeneration to cancer nanomedicine. Advanced Materials, 23(44), 5177-5218.

Wang, C.Z., Chen, S.M., Chen, C.H., Wang, C.K., Wang, G.J., Chang, J.K., Ho, M.L. 2010a. The effect of the local delivery of alendronate on human adipose-derived stem cell-based bone regeneration. Biomaterials, 31(33), 8674-83.

Zargarian, S.S., Haddadi-Asl, V. 2010. A nanofibrous composite scaffold of PCL/hydroxyapatite-chitosan/PVA prepared by electrospinning. Iran Polym J, 19, 457-468.

CHAPTER 2 IN VITRO AND IN VIVO CHARACTERIZATION OF PENTAERYTHRITOL TRIACRYLATE-CO-TRIMETHYLOLPROPANE NANOCOMPOSITE SCAFFOLDS AS POTENTIAL BONE AUGMENTS AND GRAFTS

2.1. Introduction

For the past several decades, the standard treatment to augment or accelerate bone regeneration has been the implantation of bone grafts. (Pallua & Suscheck, 2010a) Allogeneic bone grafts are costly, require time-consuming bone banking procedures, and have the potential for disease transmission. Autogenous bone grafts have long been used as bone replacements but require additional surgeries, which increase the risk of donor site morbidity and the burden on health care providers. (Ahlmann et al., 2002) Moreover, these techniques do not address the need for a clinically convenient and biodegradable method for conformally filling a critical sized bone defect while providing mechanical support and biological cues necessary to promote bone regrowth. Artificial composite scaffolds, whether bioderived, synthetic or hybrids, while studied extensively as alternatives for bone grafting and augmentation, have yet to see wide clinical adoption. (Zanetti et al., 2013b) Composite structures with calcium phosphates and magnesium silicates composing the bioactive ceramic portion, have been studied thoroughly to improve both the mechanical and osteogenic properties of scaffolds but an in situ polymerizing biodegradable bone augment or graft with biomimetic morphology and mechanical properties remains elusive. (Bohner, 2010; Hutmacher, 2000; Zanetti et al., 2013b) An initial study conducted by our group demonstrated the formation of a porous interconnected scaffold derived from the product of an amine-catalyzed Michael addition polymerization reaction.(Garber et al., 2013a) This thiol-acrylate reaction proceeds through a non-radical, step-growth process initiated by an

amine/acrylate co-monomer which is consumed in the reaction and incorporated into the growing polymer. Porous composite scaffolds made with this system were found to support human mesenchymal stromal/stem cell growth and to possess similar mechanical properties to cortical bone. (Sundelacruz & Kaplan, 2009)

The fabrication method of a scaffold can have a substantial impact on mechanical properties and bio-functionality by controlling porosity and interconnectivity. These factors influence cell attachment, proliferation, extracellular matrix production, and the transport of nutrients and wastes. (Degasne et al., 1999; Karageorgiou & Kaplan, 2005; Levine, 2008; Singh et al., 2009; Zanetti et al., 2012b) Solid freeform fabrication, thermal precipitation, gas foaming, and solvent casting followed by particulate leaching are the common approaches for making porous scaffolds for bone repair. (Karageorgiou & Kaplan, 2005; Levine, 2008) Except for gas foaming, these methods are not readily applicable to thermoset polymers due to their cross-linking densities and viscoelastic properties. Gas porogens and foaming apparatuses have the potential to be readily adapted to filling conformal defects in a clinical environment, similar to other surgical devices in use, such as fibrin sealant (Topart et al., 2005; Yeh & Tucker, 2005) and bone putty. (Gertzman & Sunwoo, 2000)

Herein we report on the in vitro characterization of the mechanical and osteoinductive properties of a gas foamed nanocomposite scaffold consisting of a thiol-acrylate copolymer with nanoscale hydroxyapatite (HA) inclusions. Scaffolds were prepared using a gas phase propellant and foaming agent to investigate the relationship of scaffold composition to morphology, mechanical properties, cytocompatibility, and osteogenic properties. The impact of varying HA 49 concentration in the PETA polymer on morphology is illustrated using SEM and micro-CT imaging. Mechanical testing was conducted to determine the compressive yield strength and

modulus of the material. To evaluate cytocompatibility and osteogenic activity, human adipose derived mesenchymal stromal cells (hASC) were used as a model cell type. Metabolic activity, DNA content, calcium deposition, and the expression of the osteogenic markers alkaline phosphatase (ALP) and osteocalcin (OCN) were quantified with respect to scaffold composition. A six-week in vivo study was also conducted to assess the basic biocompatibility of the foamed composite and the feasibility of in situ foaming for a boney fusion model.

2.2 Materials and Methods

2.2.1 Preparation of thiol-acrylate materials

All chemicals were used as received: Trimethylolpropane tris (3-mercaptopropionate) (TMPTMP) was obtained from Aldrich, diethylamine (99% purity) (DEA) from AGROS organics, and pentaerythritol triacrylate from Alfa Aesar.

Scaffolds were prepared by formulating PETA with 16.1% DEA and adding TMPTMP in a 1:1 molar functionality ratio, followed by mixing with a stir rod for 3 hours as previously described.(Garber et al., 2013a) Several concentrations of copolymer PETA with HA were studied, the first number in the abbreviation connotes the polymer content while the second number provides the amount of HA found in the composite as a wt/wt percentage (100:0, 85:15, 80:20, 75:25). The mixtures were cast into cylindrical molds (5 × 10 mm) to form a solid scaffold. The foamed composite copolymer was prepared by pouring the PETA and HA (150 g in total) into a 250 mL pressurized canister using 7 g-compressed nitrous oxide as a gas foaming agent. The foamed composite copolymer was expelled into the same cylindrical molds used for solid casting.

2.2.2 Mechanical testing

Solid and foamed scaffolds, molded to 6 mm (diameter) × 12 mm (height) cylinder shape, were tested to determine maximal compressive strength and modulus. All scaffolds, solid, gas foamed or thermally precipitated, were subjected compression, and the ultimate compressive strength was reported at 30 percent strain. A universal testing machine (Instron Model 5696, Canton, MA, USA) was used at an extension rate of 0.5 mm/min. (Garber et al., 2013a)

2.2.3 Morphological analysis

All of the scaffolds were placed on the EMS550X sputter coater, which applied a conductive platinum coating for 4 minutes followed by standard SEM analysis. Human cadaver bone from knee area was obtained under LSU exempted IRB protocol HE 13-10 from the LSU Health Science Center.

2.2.4 Micro-CT analysis

Four PETA:HA (100: 0), (85:15), (80:20), (75:25) foams were fabricated by pressurized extrusion foaming and prepared as previously described.(Garber et al., 2013a) The imaging was conducted at the Center for Advanced Microstructures and Devices (Louisiana State University, Baton Rouge, LA) using a tomography beamline with 13 keV monochromatic x-rays with a 2.5 μm/px resolution. Projection exposure time varied from 2-4 seconds with $\Delta\theta$=0.25 corresponding 51 to the number of image slices (520). Reconstruction data were 16-bit signed integer with mean air intensity scaled to zero.

Avizo 7.0.1 (Visualization Services Group) generated the volume renderings from the 3D data of the four foamed samples with two overlapping sub-volumes displayed simultaneously. The blue-green colormap represents the hydroxyapatite inclusions, and the red-orange colormap represents the copolymer foam. Image J generated 2-D orthogonal slices possessing grey colormap settings using the same data with a scale equivalent to the 3-D rendering. An

approximate pore size was also measured using Image J. The orthogonal and micro-CT datasets were directly comparable, both as an aggregate dataset and as slices.

2.2.5 Porosity calculation based on micro-Ct

To analyze the three-dimensional data, two dimensional slices were read into a custom MATLAB code. For each slice the grayscale image was thresholded using Otsu's method (Otsu, 1975) and then converted into a binary image. Morphological operations were performed to remove small imaging artifacts, and isolate interior and exterior pores. After quantifying solid and void pixels, porosity was calculated as follows:

$$\varphi = \frac{V_{pores}}{V_{pores} + V_{solid}} \times 100\%$$

2.2.6 Adult stem cells isolation and culture

Liposuction aspirates from subcutaneous adipose tissue were obtained from three healthy adult subjects (male = 1 and females = 2) undergoing elective procedures. All tissues were obtained with informed consent under a clinical protocol reviewed and approved by the Institutional Review Board at the LSU Pennington Biomedical Research Center and used under an exempted protocol at LSU A&M College. Isolation of hASCs was performed as published.(Zanetti et al., 2012b) Passage 2 of each individual was used for in vitro hASCs osteogenesis evaluation on tissue culture treated plastic or on scaffolds of different compositions. In both cases, hASCs were cultured in either stromal (control - DMEM, 10% FBS, and 1% triple antibiotic solution) or osteogenic (DMEM, 10% FBS, 0.1 μM dexamethasone, 50 μM ascorbate-2-phosphate, 10 mM β-glycerophosphate, and 1% triple antibiotic solution) media for up to 21 days with media maintenance performed three times a week.

2.2.7 hASCs loading on scaffolds and culture

All types of scaffolds were either molded or sculpted into 5 mm (diameter) × 10 mm (height) cylinder shape and gas sterilized afterwards. All the scaffolds were then submerged in stromal medium for 1 hour before loading the hASCs. The same amount of second cell passages from all donors (n = 3) were pooled and directly loaded on a single face of each scaffold type at a concentration of 1.0 × 104 cells/μL for total volume of 5 μL. After 30 min of incubation in a saturated humidity atmosphere incubator at 37 °C and 5% CO2, the same volume of hASCs containing solution were directly applied on the opposite side of each scaffold as previously described. (Zanetti et al., 2012b) Control groups included PCL:HA (100:0 and 80:20) scaffolds. Experimental groups included PETA:HA (100:0, 85:15, 80:20, 75:25) scaffolds. Scaffolds loaded with hASCs were immediately transferred to 48-well plates and cultured in stromal or osteogenic media for 21 days. Cell medium were changed every 2-3 days. Triplicates were performed for each assay.

2.2.8 In vitro hASC metabolic activity on scaffolds

AlamarBlue™ (Life Technologies) is a useful measure of metabolic activity and is frequently used as an analog of cell viability and proliferation. All scaffold samples were seeded with hASC and cultured in stromal or osteogenic media for 21 days. The AlmarBlue™ conversion was measured at 7, 14, and 21 days The scaffolds were removed from culture, washed three times in Phosphate Buffered Saline (PBS), and incubated with 10% Alamar Blue™ in Hank's balanced salt solution (HBSS) without phenol red (pH 7) for 90 min. The fluorescence of three aliquots (100 μL) from each scaffold were measured at an excitation wavelength of 530 nm and an emission wavelength of 595 nm using a fluorescence plate reader (Wallac 1420 multilabel hts counter).

2.2.9 Alizarin red staining

hASCs calcium deposition (triplicates of scaffolds alone and cell-scaffolds) was assessed after 7, 14, and 21 days of culture in control or osteogenic medium based on alizarin red staining. Wells were washed with 0.9% NaCl and fixed with 70% ethanol. Wells were stained with 2% alizarin red for 10 minutes and washed with DI water. Wells were destained with 10% cetylpyridinium chloride monohydrate for 4 hours at room temperature with constant agitation. Results were normalized to values from scaffolds cultured without cells for the same time periods.

2.2.10 In vitro quantification of DNA on scaffolds

Total DNA content was used to determine the number of cells on each scaffold as previously described.(Liu et al., 2008a) After triplicates of each scaffold were minced by a scalpel and the DNA was digested with 0.5 mL of 0.5mg/mL proteinase K (Sigma-Aldrich) at 56 ºC overnight, 54 aliquots (50 µL) were mixed with equal volumes of 0.1 g/mL Picogreen dye solution (Invitrogen) in 96-well plates. Samples were then excited at 480 nm with a plate reader (Wallac 1420 multilabel hts counter). Scaffolds without cells were used as negative controls.

2.2.11 Quantitative real-time polymerase chain reaction (QPCR)

Total RNA was extracted from triplicates of cell-scaffold constructs as previously described.(Zanetti et al., 2012b) Total RNA to cDNA EcoDry Premix (ClonTech) for cDNA synthesis. qRT-PCR was performed using 2× iTaqTM SYBR® green supermix with ROX (Biorad) and primers for alkaline phosphatase (ALP) and osteoscalcin (OCN)(Zanetti et al., 2012b) to quantify osteogenic target gene expression of hASC loaded to scaffolds and cultured in either stromal or osteogenic media for 7, 14, and 21 days. Reactions were performed with a MJ MiniTM Thermal Cycler (BioRad). The sequences of PCR primers (forward and backward, 50-

30) were as follows: ALP, 5'-AATATGCCCTGGAGCTTCAGAA-3' and 5'-CCATCCCATCTCCCAGGAA-3';OCN, 5'-GCCCAGCGGTGCAGAGT-3' and 5'-TAGCGCCTGGGTCTCTTCAC-3'.Samples were normalized (ΔCt) against the house keeping gene 18S rRNA and the - ΔΔCt value of ALP and OCN in scaffolds cultured in osteogenic and control media was calculated using the ΔΔCt method.(Livak & Schmittgen, 2001b)

2.2.12 Statistical analysis

All results were expressed as mean ± SEM. Data was analyzed with one-way analysis of variance (ANOVA), followed by Tukey's minimum significant difference (MSD) post hoc test for pairwise comparisons of main effects. For all comparisons, a P-value < 0.05 was considered significant.

2.2.13 In vivo study

Scaffold Preparation and Surgical Implantation

Five male Fischer rats (Harlan Sprague-Dawley, Indianapolis, IN) were randomly assigned to three different treatments: (1) 1 rat was implanted with pre-sculpted PETA+20% HA, (2) 3 rats were implanted with PETA+20% foamed in situ, or (3) 1 rat was implanted with PETA+0% HA foamed in situ Stock/HA and TMPTMP/HA pre-polymer mixture were placed into a 250 mL pressurized spray canister with 7 g-compressed nitrous oxide as a gas foaming agent. The foamed composite copolymer was expelled from the canister onto a sterile surface. The solid composite was cut into a rectangle with dimensions (15 mm × 10 mm × 1 mm) for rat number 1. For rats 2, 3, and 4, the pre-polymer mixture was prepared as described above and foamed into a 5 mL syringe for surgical application. The process was the same for rat 5, but the formulation did not contain HA. The rat posterolateral lumbar spinal fusion surgery was performed as previously described (Aust et al., 2004). Prior to general anesthesia, rats received a

subcutaneous injection of 0.5 mg/kg butorphanol (Torbugesic, Fort Dodge Animal Health) and 0.02 mg/kg glycopyrrolate (Robinul-V, Fort Dodge Animal Health, Fort Dodge, IA). Isoflurane was administered 20 minutes later in an induction chamber to induce anesthesia. The isoflurane was maintained at 1.5% via nose cone on a Bain circuit for the remainder of the procedure. The lumbar region was clipped and aseptically prepared with 70% isopropanol and betadine. A posterior midline skin incision was made over the lumbar spine. Two fascial incisions were made 3 mm lateral and parallel to the dorsal spinus processes. The L4 and L5 transverse processes were exposed with sharp and blunt dissection. A scalpel was used to decorticate each transverse process. Surgical sites were thoroughly lavaged with physiologic saline. In rat 1, solid scaffolds 56 were placed adjacent to both sides of the spine such that they spanned between the midpoint of each transverse process. For the remaining rats, 3 ml of each foamed scaffold was applied so that scaffold spanned between the center of each transverse process next to the spine. Fascial and subcutaneous incisions were closed separately with 3-0 polyglactin 910 (Vicryl, Ethicon) in a simple continuous pattern. Closure of the fascia around the implants effectively filled any potential space. A subcutaneous/subcuticular suture pattern was used to approximate skin edges, and tissue adhesive was used for skin closure (Vetbond, 3M). Scaffolds were harvested 3 (rat 3) or 6 (rats 1,2,4,5) weeks after implantation following euthanasia by CO_2 asphyxiation (Lopez et al., 2009). At 3 weeks, no significant results were shown in radiographs, micro-CT or histology analysis. Therefore, no results from Rat 3 were reported in the results and discussion sections.

Micro-CT Analysis

Immediately postmortem, two-dimensional (2-D) microcomputed tomography (μ-CT) imaging was performed (40 kV and 540 ms) to obtain 0.04 mm slices every 0.9°throughout a 360° rotation (SkyScan 1074, Skyscan n.v., Belgium). Three-dimensional (3-D) files were

reconstructed from 2-D images. Measurements of 2-D and 3-D images were performed with AVIZO® Standard packages (FEITMVisualization Sciences Group). A density line was first drawn in void space with no tissue to measure the optical density (OD) of the image background. The line was then moved to L3 of the specimen's vertebral column to determine the OD of the tissue unaffected by the surgery. Lastly, the density line was moved between L4 and L5 of the specimen's vertebral column to calculate the OD of the area treated by the scaffolds. The density of the area treated by the implant was normalized by the densities of the void space and the unaffected bone region in order to calculate the percentage of bone growth present in each specimen (Lopez et al., 2009).

$$OD = \log \frac{255}{pixel\ value} \qquad \frac{OD_{Treated}}{OD_{Untreated}} \times 100 = \%\ new\ growth$$

Histology

Following imaging, spines were cut in half and fixed in neutral buffered formalin. One half of each spine was decalcified, paraffin embedded and longitudinal sections (5 um) were stained with hematoxylin and eosin. Microarchitecture was evaluated using Olympus BX46 microscope.

2.3. Results

2.3.1. SEM analysis

The foamed scaffold samples were analyzed using SEM to examine the trends in morphology. The morphology of the foam containing 0-20% HA was similar to cancellous human cadaver bone (Figure 2.1).

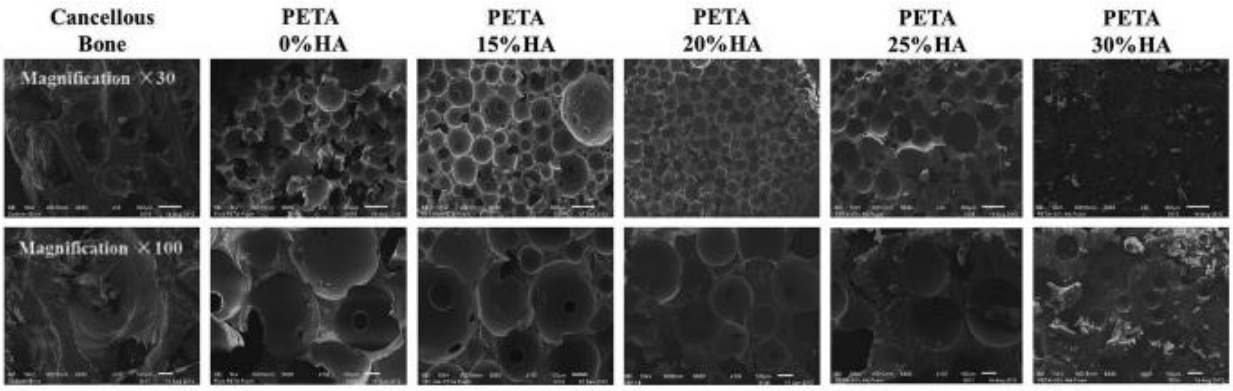

Figure 2.1 SEM analysis of PETA:HA (100:0), (85:15), (80:20), (75:25) scaffolds

The average pore diameters of PETA: HA 100:0 and 85:15 scaffolds were 250µm-300µm, with no significant difference between the two. PETA:HA 80:20 had a slightly smaller pore diameter of 150µm-200µm. The pore diameter of PETA:HA 75:25 was only 70µm-100µm. PETA:HA 70:30 had a pore diameter of less than 50µm. It is apparent from the results in Figure 2.1 that pore size is inversely related to HA content; pore diameter decreases as HA concentrations increase. Additionally, increasing HA content correlates with increased pore wall thickness and an apparent reduction in scaffold interconnectivity.

2.3.2. Micro-CT analysis and porosity calculation

There is a limitation associated with the amount of material that SEM can qualitatively analyze, reducing the generalizability of the data. To address this limitation, the interconnectivity, pore volume, and ceramic phase distribution of HA-PETA copolymer composites and PCL (control) were further analyzed by micro-CT. Micro-CT image analysis is a more senstivie method for estimating porosity of materials when compared to SEM, flow porosimetry, and gas adsorption. (Ho & Hutmacher, 2006) Volume renderings (Figure 2.2) were generated from PETA and PCL composite foam 3-D data using Avizo 7.0.1 (Visualization Services Group). Two overlapping sub-volumes were rendered simultaneously, one with a red-

orange-white colormap corresponding to thiol-acrylate foam, and another with a blue-green colormap corresponding to hydroxyapatite additives. The porosity of PETA: HA (100:0, 85:15, and 80:20) are 66.9%, 72.0%, and 66.4% respectively (Figure 2.3A). It should be noted that an apparent transition in morphology occurred between 20% and 25% HA inclusions. As HA concentration increased from 20% to 25%, the porosity decreased significantly from 66.4% to 44.7%. When HA concentration reaches 25%, the pore size is substantially reduced and the interconnected void volume appeared to decrease, resulting in a structure similar to a closed-cell foam (Figure 2.2K&L).

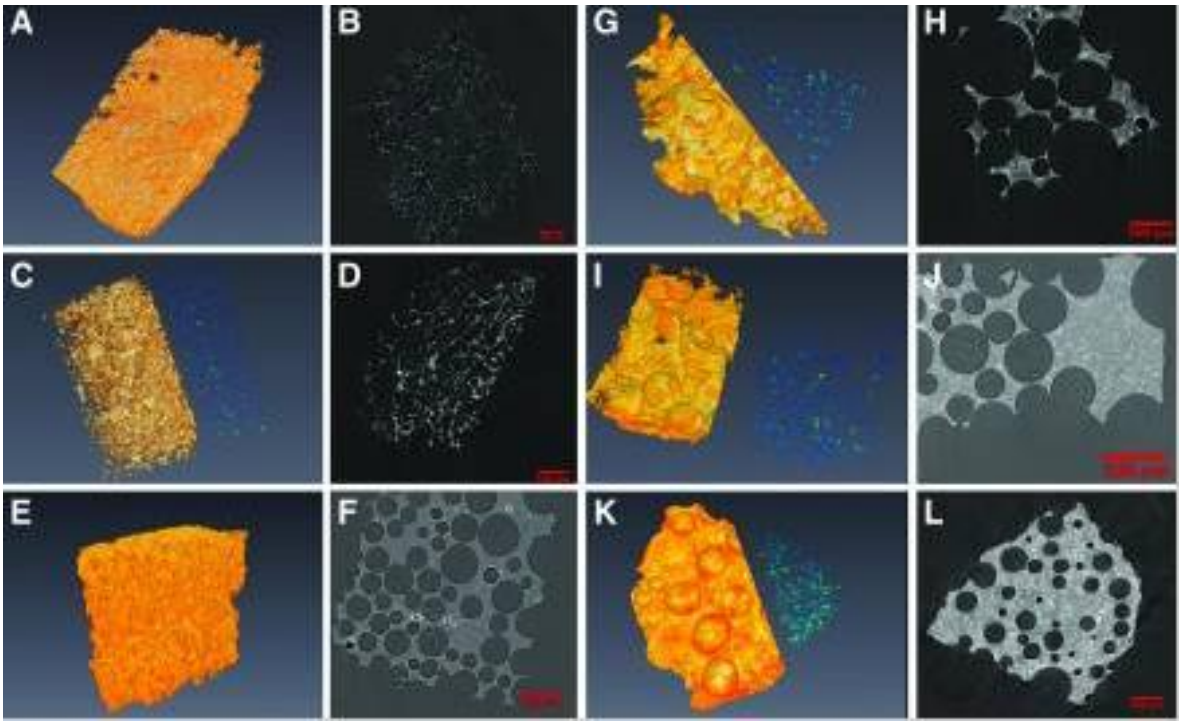

Figure 2.2 Avizo rendering pictures (3D &2D) of micro-ct data of scaffolds. Figure 2A & 2B PCL:HA (100:0); Figure 2C & 2D PCL:HA (80:20) ;Figure 2E & 2F PETA: HA (100:0) Figure 2G & 2H PETA: HA (85:15) scaffolds; Figure 2I & 2J PETA: HA (80:20) scaffolds; Figure 2 K & 2L PETA: HA (75:25) scaffolds. Each scale bar in the 2D pictures indicates 500μm.

This is attributed to increased polymer solution viscosity correlated with reduced N2O expansion and mobility. In addition, the inclusion of 20% HA to PCL scaffolds increased the porosity from 78.0% (PCL:HA 100:0) to 87.6% (PCL:HA 80:20) (Figure 2.2A & 2.2C).

2.3.3. Mechanical testing

Figure 2.3B shows the compressive yield strength of the foamed and solid PCL:HA (100:0, 80:20), PETA:HA (100:0, 85:15, 80:20, 75:25) samples.

Compressive strength of solid PCL:HA (100:0, 80:20) samples are significantly higher than corresponding PETA:HA (100:0, 80:20) samples. When comparing among porous scaffolds, PETA:HA (100:0, 80:20) scaffolds are either the same as or stronger than PCL:HA (100:0, 80:20). The compressive strength of the foamed PETA:HA steadily increased with increasing HA content; however, the solid samples did not follow a similar trend. The addition of 15% HA in the foam resulted in a significant increase in compressive strength compared to the control samples and increasing the HA content beyond 15% correlated with increased compressive strength.

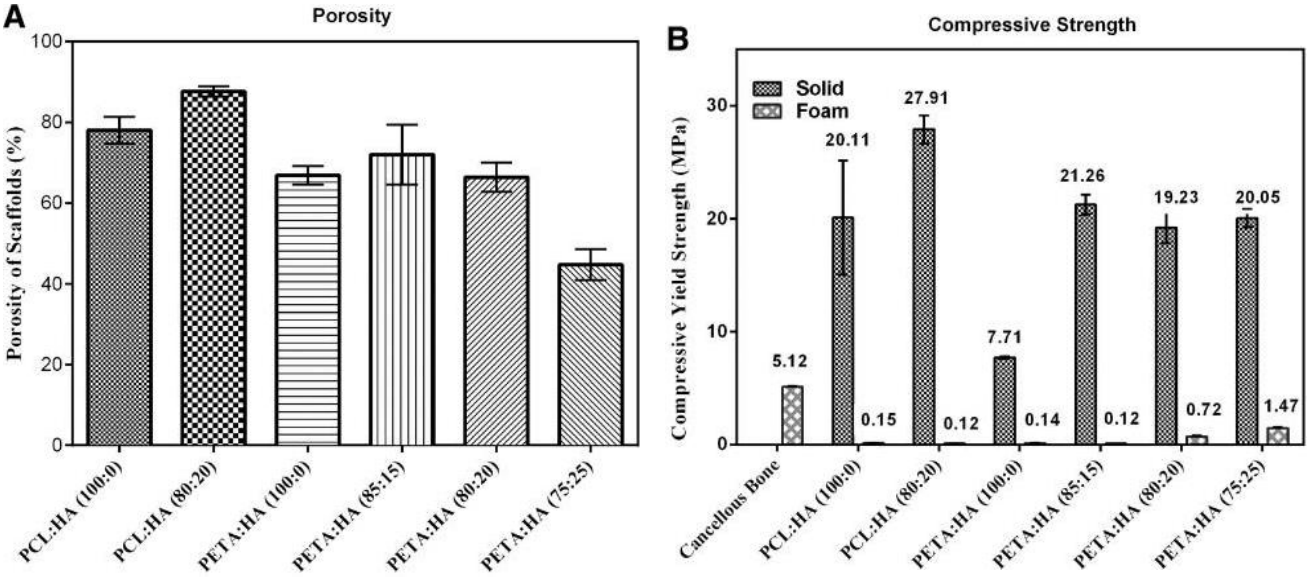

Figure 2.3 porosity of PETA:HA (100: 0), (85:15), (80:20), (75:25) scaffolds; B: maximum compressive strength of PETA:HA PETA:HA (100: 0), (85:15), (80:20), (75:25) composites(solid and foam)

Conversely, solid PETA:HA (85:15, 80:20, 75:25) composite scaffolds exhibited approximately the same compressive strength for all HA containing samples. It is believed that the porosity (Figure 2A) is responsible for the different trends between solid and foamed scaffolds.

2.3.4. hASCs metabolic activity and proliferation on scaffolds cultured in control and osteogenic media

For cell-scaffold constructs cultured in stromal media, PETA:HA (100:0) had the highest metabolic activity after 14 days of culture. PCL:HA (100:0) had the highest levels of metabolic activity after 21 days of culture in stromal medium and no significant differences were observed from this scaffolds between any time point. In osteogenic media, PETA:HA (100:0) scaffolds again exhibited the highest metabolic activity after 7, 14 and 21 days of culture. PETA:HA (85:15 and 80:20) scaffolds had the next highest metabolic activity at all time points. PCL scaffolds showed the lowest levels of metabolic activity after 7, 14 and 21 days of culture (Figure 2.4A). The addition of HA to PETA and PCL scaffolds decreased metabolic activity on constructs cultured in stromal and osteogenic media.

Significantly higher metabolic activity in was observed at all-time points for PCL:HA (100:0) and PCL:HA (80:20) scaffolds cultured in stromal media compared to osteogenic media. This data is in agreement with previous studies which indicate the metabolic activity of hASC is expected to decrease as cells commit to an osteogenic linage.(Qureshi et al., 2013; Zanetti et al., 2012b)

No differences in metabolic activity were seen in PETA:HA composite samples between stromal and osteogenic conditions. hASCs cultured on HA-containing scaffolds were expected to begin differentiation into an osteogenic linage regardless of the media condition, potentially accounting for the differences in metabolic activity between HA-containing and control samples with respect to media condition. Almost no metabolic activity was measured in PETA:HA (75:25) scaffolds, likely as a result of the reduced pore size and interconnectivity.

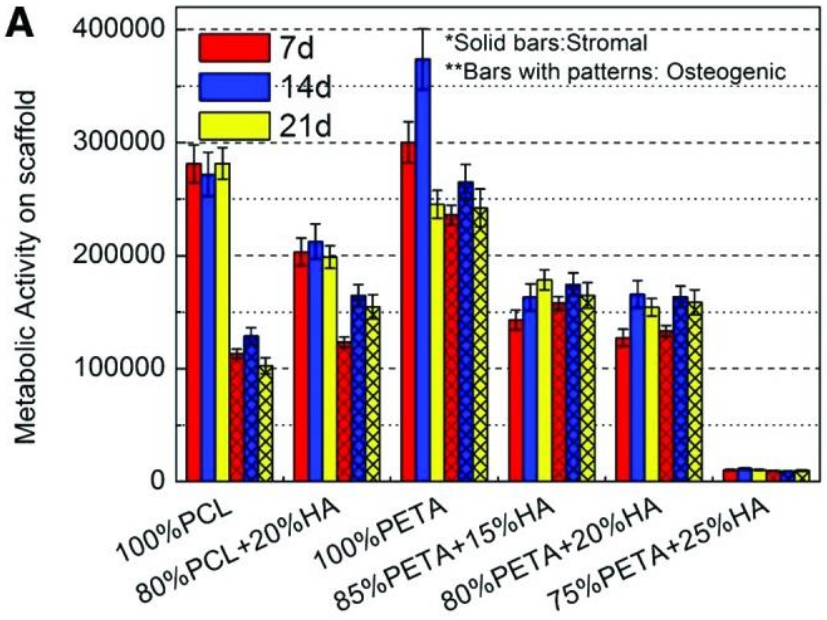

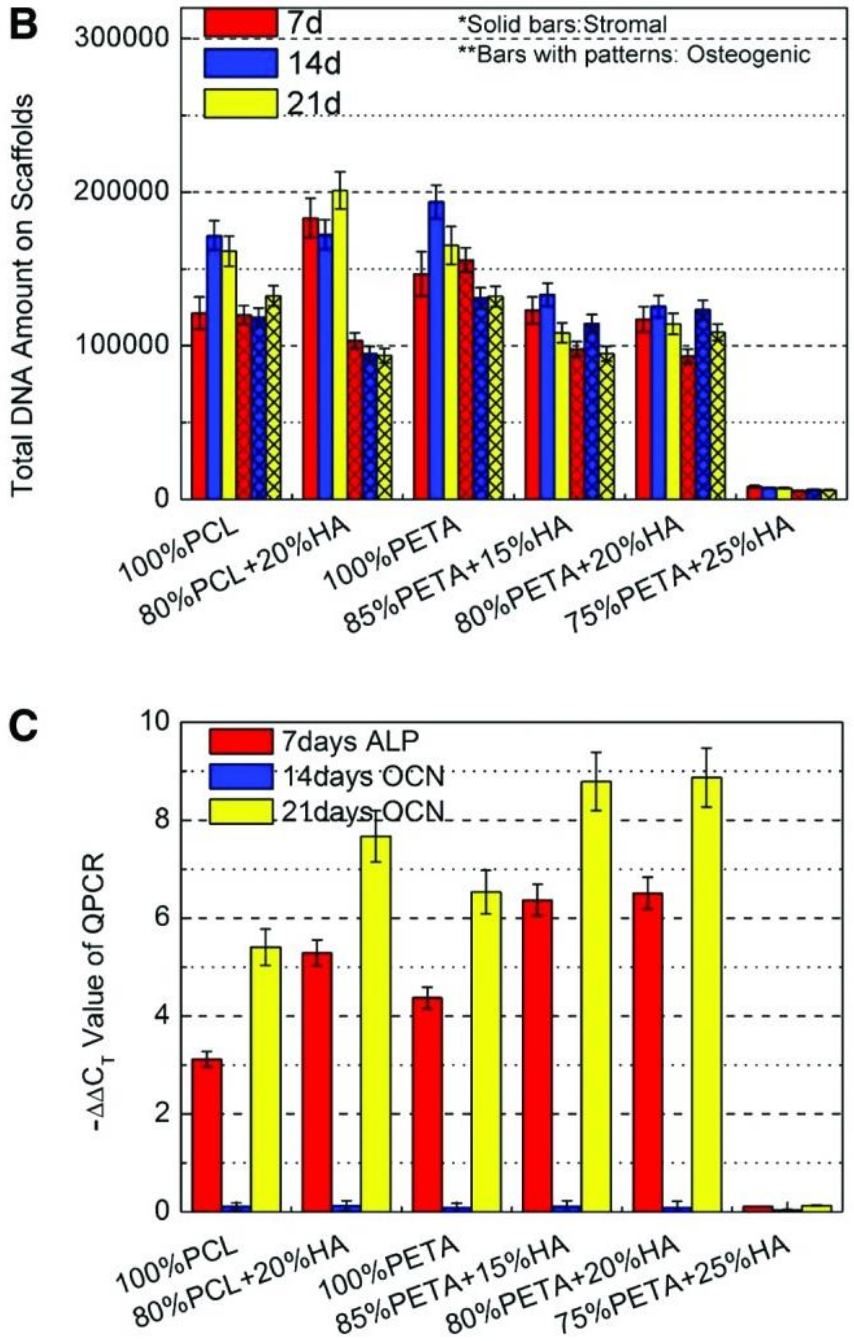

Figure 2.4 Panel A: relative metabolic activity of hASC on PETA:HA (100:0), (85:15), (80:20), (75:25) scaffolds; Panel B: relative DNA content of hASC on PETA:HA (100: 0), (85:15), (80:20), (75:25) scaffolds; Panel C: q-rtPCR analysis of ALP (7 day) and OCN (14 and 21 day) expression from hASCs on PETA:HA (100:0), (85:15), (80:20), (75:25) scaffolds.

Total DNA content was quantified using Quant-iT™ PicoGreen ® , to analyze the hASC proliferation in scaffolds. Differences in DNA content, between stromal and osteogenic media conditions, were observed at the 7 day culture time point for PCL:HA (80:20), PETA:HA (85:15) and PETA:HA (80:20) composite scaffolds. When comparing samples within the stromal media treatment condition, it can be observed that the PETA:HA samples had significantly fewer cells than the PCL or PETA control. The most pronounced difference in DNA content was between PCL:HA (80:20) composites and PETA:HA scaffolds in stromal media conditions, (Figure 2.4B) where the DNA content in PCL (80:20) scaffolds was significantly higher than PETA:HA composites. At 14 and 21 days, levels of DNA content observed in both PCL scaffolds and the pure PETA scaffolds were significantly higher than the PETA:HA composites, in stromal media conditions. Within the osteogenic media treatment groups, the PETA:HA scaffolds showed slightly increased DNA content compared with the PCL:HA scaffolds, but all scaffolds contained a similar numbers of cells.

2.3.5. Quantitative real-time polymerase chain reaction (QPCR)

Bone morphogenic proteins (BMPs), known to regulate osteogenesis, act on the transcription factor core binding factor alpha1 (Cbfa1) and result in the activation of osteoblast-related genes, such as ALP and OCN. (Liu et al., 2008a; Milat & Ng, 2009) The expression of these genes are commonly used as early and middle stage markers of osteogenesis, respectively.(Burge et al., 2007) QPCR was used to assess the expression of ALP at the 7 day time point and OCN at 14 and 21 day time points (Figure 2.4C). Based on previous studies, ALP expression in hASC decreased dramatically after 7 days in culture and was therefore not measured at the 14 and 21 day time points in this study.(Burge et al., 2007; Zanetti et al., 2012b) The differences in the 64 expression of ALP and OCN in hASCs cultured on scaffolds in stromal

and osteogenic media are represented in Figure 2.4C. The cells on PETA:HA (85:15) and PETA:HA(80:20) scaffolds showed similar expression of ALP at 7days and were significantly higher than all other PETA and PCL scaffolds. Additionally, hASC on pure PETA scaffolds had higher ALP expression than pure PCL control scaffolds. While hASC cultured on PCL:HA(80:20) scaffolds had higher ALP expression than pure PETA or PCL, the expression was still lower than PETA:HA (85:15) and PETA:HA(80:20) scaffolds. Moreover, the expression of the OCN marker could only be observed at 21 days of culture, with little expression at 14 days regardless of treatment. The OCN expression level demonstrated in hASC as a function of scaffold type was the similar to that of ALP expression with maximal OCN expression observed in PETA:HA (85:15) and PETA:HA(80:20) followed closely by OCN levels in PCL:HA composites. Consistent with the previously described results, cells cultured on the PETA:HA (75:25) sample did not demonstrate substantial expression of either marker, likely the result of poor cell proliferation/survival associated with the lack of a porous and interconnected structure.

2.3.6 Calcium deposition in hASCs cultured in control and osteogenic media

The mineralization of different scaffold types was assessed using alizarin red staining, which stains calcium-rich deposits. hASC cultured on the PETA composites in stromal and osteogenic media were tested against PCL and PCL:HA scaffolds. (Figure 2.5A)

As expected, alizarin red staining was significantly higher in hASC cultured in osteogenic media compared to samples cultured in stromal media. (Zanetti et al., 2012b) Also, hASC cultured in osteogenic media showed a significant increase in staining with respect to increased 65 time in culture. Except for PETA:HA (75:25), all scaffolds showed significant differences in the calcium deposition at 14 days between stromal and osteogenic media.

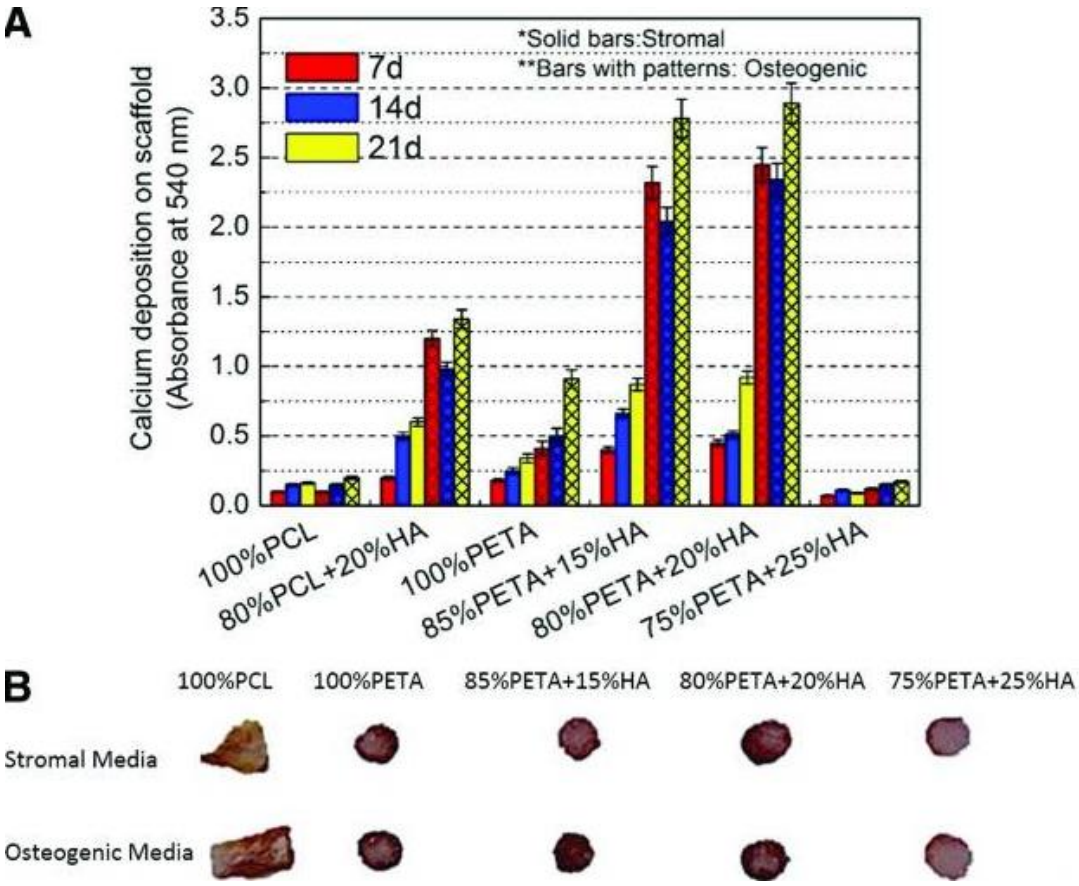

Figure 2.5 Alizarin red stain of PETA:HA as a function of scaffold composition, media treatment and time. Panel A, quantitative analysis of staining on scaffolds loaded with hASC and cultured in stromal and osteogenic media for 7, 14 and 21 days. Panel B, cross section of each type of scaffold stained with alizarin red on 21 days.

Both PETA: HA (80:20) and PETA:HA (85:15) cultured in osteogenic media demonstrated significantly increased staining compared to all other experimental samples and controls. Almost no calcium deposition, however, was observed at 14 and 21 day culture time points in PETA:HA (75:25).

2.3.7 In vivo study

Radiography

Observed behavior and weight gain were normal (90.7 ± 5.9 g) for all rats after surgery. Foamed thiol-acrylate nanocomposite implants showed some increase in radiographically detectable opacity 3 weeks after implantation compared to immediately after surgery, and the opacity increased further by 6 weeks after implantation. The increasing intensity of bone scaffolds is consistent with scaffold calcification (Figure 2.6). Rats implanted with pre-molded samples, had a lower increase in radioopacity by 6 weeks after implantation compared to rats implanted with PETA+HA foamed *in situ*.

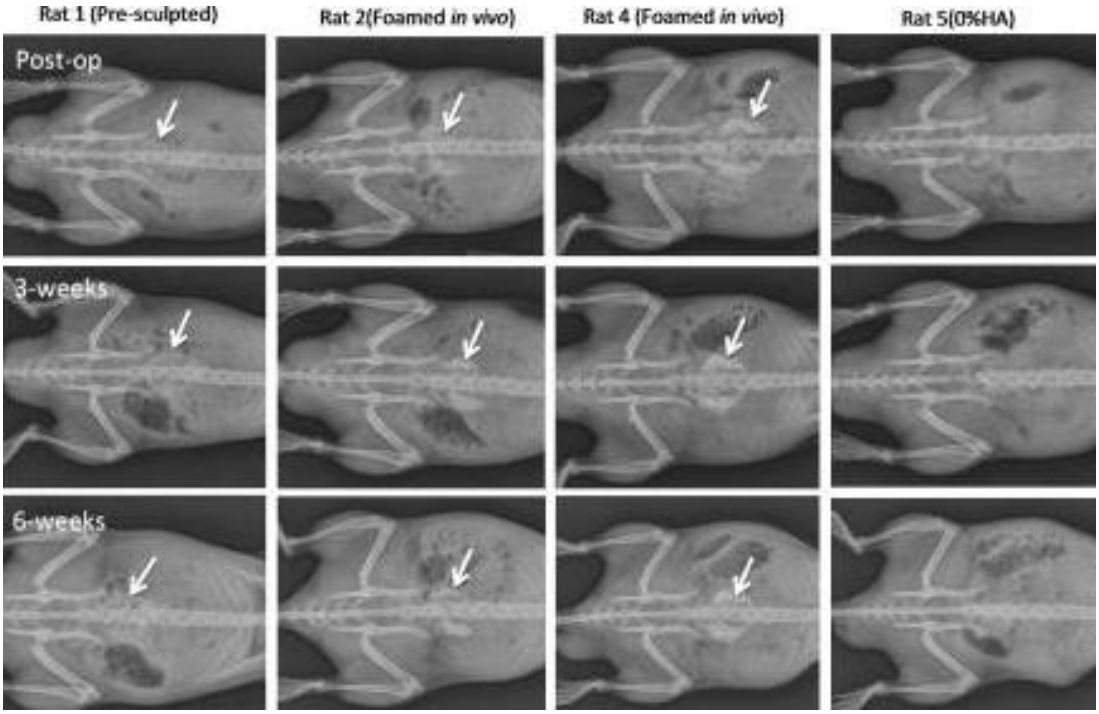

Figure 2.6 Radiographs of in vivo study

No evidence of calcification was observed in implants of 0% HA pre-sculpted PETA. This is consistent with the in vitro osteogenesis target gene expression results.

Microcomputed Tomography

The micro-CT results support the radiographic findings. The light colored regions indicate densification in the scaffolds in Figure 2.7. *In vivo, in situ*-polymerized scaffolds had the greatest amount of densification six weeks after surgery.

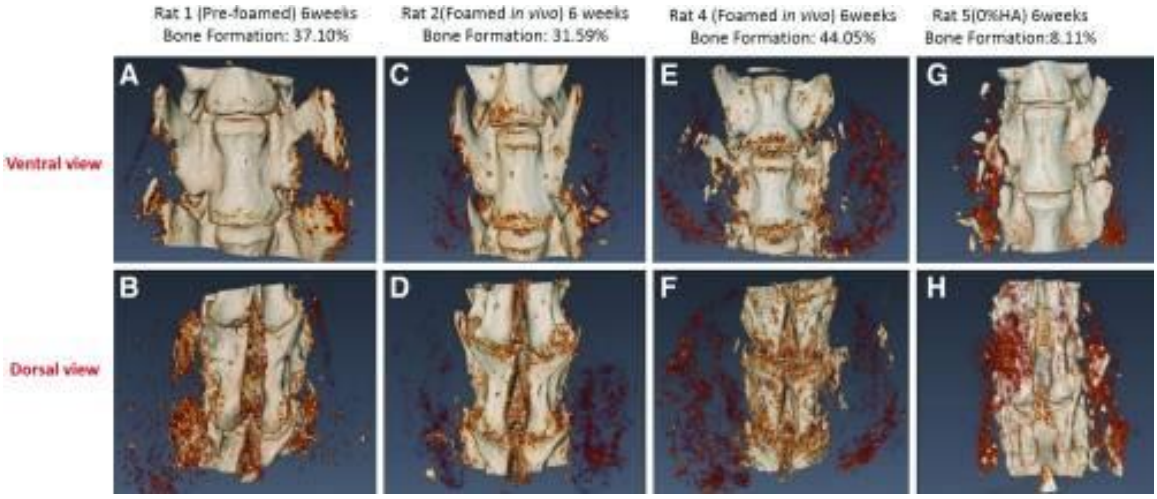

Figure 2.7 Micro-CT data of the L4 (top) and L5 (bottom) vertebral bodies from the in vivo study. The light colored regions indicate densification in scaffolds.

Analysis of Bone Formation using histology

Histological examination was performed on pre-sculpted PETA:HA (80:20), PETA:HA (80:20) foamed in situ, and PETA:HA (100:0) foamed *in situ*. The essential step of decalcifying and staining the spinal column poses a problem in analyzing tissues for bone formation evaluating the calcified areas. For this reason, tissue morphology is considered a reliable parameter to measure bone formation(Schulte et al., 2013). Each cohort was examined six weeks post-op.

Treatment cohort 1 (pre-sculpted PETA:HA (80:20) proved to be biocompatible, support cell growth, and induce osteogenesis in tissue growing into the foam structure. Figure 3.8A shows that the PETA:HA (80:20) implant is partially demarcated by fibrosis and multifocal fibrocartilage formation, which incorporates multifocal, small areas of endochondral ossification.

Figure 3.8D contains the implant surrounded by fibrous tissue, fibrocartilage, and peripheral endochondral ossification. The appearance of cells chondrocytic in appearance, a tide mark, and an ossified site present around the implant site indicate that the PETA:HA (80:20) scaffold have the potential to induce endochondral ossification.

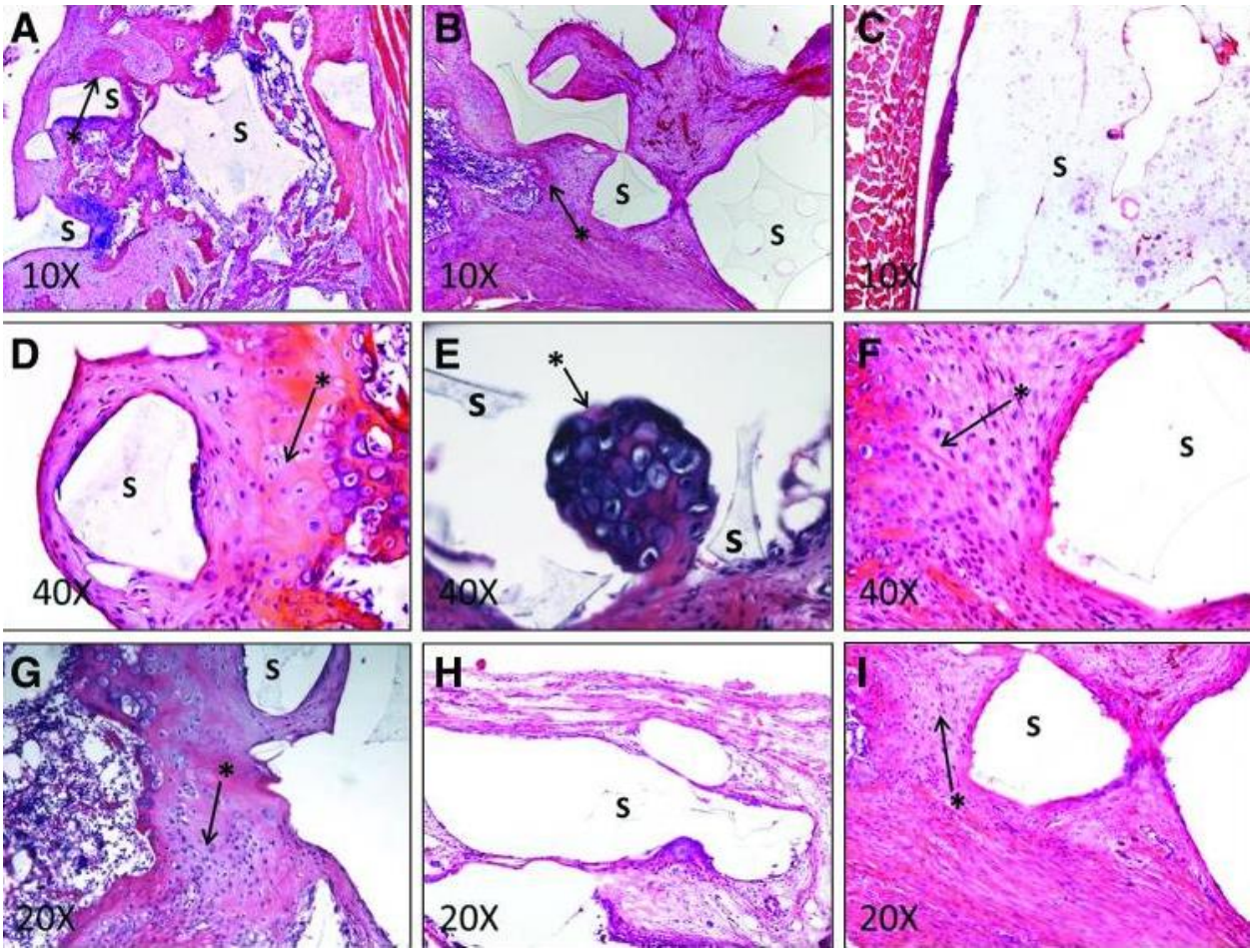

Figure 2.8 Histology analysis using Hematoxylin and eosin staining. A medial cut was made on the spinal column of each rat. The progress of this specimen guides the analysis of the other specimens. Figures 8A, 8B, 8D, 8F, and 8I: Rat was treated with the pre-sculpted PETA:HA (80:20) scaffold. Figure 8C, 8E, and 8G: Rats were treated with PETA:HA (80:20) scaffold foamed in situ. Figure 8H: Rat was treated with PETA:HA (100:0) foamed in situ. S: scaffold implants; *: site endochondral ossification

Figure 2.8B shows that the polymer implant is segmentally demarcated by fibrous and fibrocartilagenous tissues with an ossified rim blending into pre-existing trabecular bone. The findings in Figure 2.8B are further supported by Figure 2.8I and Figure 2.8F.

Treatment 2 (PETA:HA 80:20 in situ) was also shown to be biocompatible, support bone growth, and induce osteogenic differentiation. In cohort 2, histological changes are characterized by ostegenic activity around the implant site. Figure 2.8C shows a large accumulation of polymer implant near the skeletal muscle of the rat, surrounded by a thin layer of fibrous tissue with a focal area also containing macrophages. Figure 2.8E shows the presence of a cavitation lined by 1-3 layers of spindled cells (fibroblasts) containing the scaffold and a sprouting nidus of endochondral ossification. Figure 2.8G shows that in the area adjacent to the polymer-occupied cavitation, there are fibrous tissues and a region of endochondral ossification.

Histological analysis of cohort 3 PETA:HA (100:0) indicates that the lack of nanoscale HA reduces the osteogenic properties of the scaffolds. In Figure 2.8H, the scaffold is surrounded by a very thin layer of fibrous tissue, indicating a reduction in the formation of organized tissue in the implant region.

2.4. Discussion

Bone tissue engineering involving polymer/ceramic composites presents an attractive alternative approach to the repair and regeneration of damaged or traumatized bone tissue. (Gaalen et al., 2008; Pallua & Suscheck, 2010b). Several studies have previously explored the potential use of thiol-acrylate chemistry for biomedical devices, but radical based photoinitiators are usually used to drive the polymerization process.(Rydholm et al., 2008; Rydholm et al., 2006; 70 Zanetti et al., 2012b) A non-radical based polymerization method is potentially less cytotoxic and therefore more amenable to in situ polymerization. The amine catalyzed Michael

addition for thiol-acrylate polymerization described in this study has potential advantages compared to photoinitiated reactions because the chain propagation does not require a free radical initiator during the polymerization reaction. The mechanism of this amine-catalyzed reaction has been previously investigated.(Bounds et al., 2013; Garber et al., 2013a) The general reaction occurs via the formation of a catalyst/comonomer molecule by the Michael addition of a secondary amine across the alkene end group found in acrylate monomers. The in situ catalyst produced reacts with a trifunctional thiol and trifunctional acrylates forming a high-density cross-linked copolymer. The step growth nature and the incorporation of the tertiary amine catalyst reduce concerns about potential leaching of free radical initiators and unreacted monomer. This reaction, therefore, is potentially more attractive for in situ polymerization for bone formation than comparative free radical-based methods.

The PCL-based scaffold was synthesized via a thermal precipitation method resulting in pore size, volume, and interconnectivity that are largely independent of solution viscosity.(Qureshi et al., 2012) Results showed that such characteristics were directly influenced by the viscosity of the stock solution in the polymerization of PETA composites. (Barby & Haq, 1985). It is well documented that an interconnected pore structure can help support cell migration, cell differentiation, nutrient transport (Di Maggio et al., 2011; Lawrence & Madihally, 2008) and, in some cases, formation of blood vessels. (Mehrkens et al., 2009; Papadimitropoulos et al., 2011; Scherberich et al., 2007) Because HA was found to decrease interconnectivity, it was expected that the highest HA concentration sample, PETA:HA (75:25), would not provide a suitable environment for cell in-growth and nutrient/waste transport. Electron microscopy images and micro-CT analysis indicate PETA:HA (75:25) scaffolds lack interconnectivity of the void volume providing for cell penetration and nutrient/waste transport required for cell growth

and differentiation. The analysis of cell viability and expression of osteogenic markers further supported this hypothesis.

The decreased metabolic activity of PETA:HA composites compared to the PETA control is likely related to differences in cell function, not cell number, attributed to osteogenic differentiation of hASC. The decreased cell proliferation and metabolic activity also had an inverse relationship with the increased calcium deposition and expression of osteogenic markers. This data further supports the hypothesis that hydroxyapatite induces osteogenesis, resulting in decreased metabolic activity and proliferation. (Bernhardt et al., 2009; He et al., 2010)

Calcium deposition correlated with the expression of ALP and OCN in hASC cultured on PETA:HA (85:15) and PETA:HA (80:20) scaffolds, which were significantly greater than PCL:HA (80:20), pure PCL, and PETA control scaffolds in both media conditions, providing a further indication that scaffolds composed of PETA may be an appropriate material for the repair of bone defects. Increased alizarin stain uptake in PETA: HA (80:20) and PETA:HA (85:15), compared to PCL:HA (80:20), does not correlate with increased cell density or metabolic activity but does correlates with increased ALP and OCN expression. PETA is better able to induce the expression of osteogenic markers than PCL, but further comparisons at differing concentrations and with other degradable resins are required to test this hypothesis. Cross sectional images of PETA:HA (75:25) scaffolds demonstrate poor alizarin red penetration providing further support that the void volume in not substantially interconnected.

Although increasing HA content resulted in reduced pore size and interconnectivity, it provided a more solid and stronger structure for the scaffold. Other studies have shown a similar trend of decreasing porosity with increasing HA content.(Zhang & Ma, 1999) The increase in compressive strength seen in solid samples is predictable and similar to that seen with other

nanoscale polymer fillers.(Ahn et al., 2004; Reynaud et al., 2001) As porosity played no role in the solid samples, the increase in viscosity with increasing HA content beyond 15% did not significantly affect the mechanical strength. Histological results demonstrated that both the presculpted and foamed in situ PETA:HA (80:20) scaffolds induced endochondral ossification. Radiography results indicating increased densification further supported these findings. During the in vivo study, the structure of the in situ polymerized foam sample may have been disrupted when the surgical site was closed during the surgery. Poor porosity and interconnectivity could be the reason why the densified regions of the radiographs were non-continuous. Overall results suggest that PETA:HA scaffolds could be a suitable substrate for bone regeneration.

2.5. Conclusion

By gas foaming thiol-acrylate based copolymers synthesized via Michael addition with an in situ amine-catalyst, a porous polymeric scaffold with bone-like morphology was developed as a potential graft or augment in critical-sized bone defect repair. Not only does PETA:HA composite have substantial porosity and interconnectivity, it also demonstrates adequate mechanical strength as compared to cortical bone. Compared to PCL:HA composites, both PETA:HA (85:15) and PETA:HA (80:20) scaffolds showed higher mineral deposition and ALP and OCN expression level. Overall, the PETA:HA had higher compressive strength and improved cytocompatibility compared to PCL controls. Mesenchymal cells cultured on PETA based scaffolds had a greater expression of osteogenic markers and the scaffolds exhibited significantly greater mineralization than hASC cultured on PCL controls. The in vivo study demonstrated that animals injected with PETA:HA composites showed no signs of surgical site or systemic toxicity and that PETA:HA composites induced osteogenesis in vivo. Additionally,

the study serves as a proof-of-concept that gas foaming of thiol-acrylate polymers in vivo may be used to conformally fill irregular sized defects.

2.6. References

Ahlmann, E., Patzakis, M., Roidis, N., Shepherd, L., Holtom, P. 2002. Comparison of anterior and posterior iliac crest bone grafts in terms of harvest-site morbidity and functional outcomes. J Bone Joint Surg Am, 84-A(5), 716-20.

Ahn, S.H., Kim, S.H., Lee, S.G. 2004. Surface-modified silica nanoparticle–reinforced poly (ethylene 2, 6-naphthalate). Journal of Applied Polymer Science, 94(2), 812-818.

Aust, L., Devlin, B., Foster, S., Halvorsen, Y., Hicok, K., Du Laney, T., Sen, A., Willingmyre, G., Gimble, J. 2004. Yield of human adipose-derived adult stem cells from liposuction aspirates. Cytotherapy, 6(1), 7-14.

Barby, D., Haq, Z. 1985. Low density porous cross-linked polymeric materials and their preparation and use as carriers for included liquids, Google Patents.

Bernhardt, A., Despang, F., Lode, A., Demmler, A., Hanke, T., Gelinsky, M. 2009. Proliferation and osteogenic differentiation of human bone marrow stromal cells on alginate-gelatinehydroxyapatite scaffolds with anisotropic pore structure. J Tissue Eng Regen Med, 3(1), 54-62.

Bohner, M. 2010. Resorbable biomaterials as bone graft substitutes. Materials Today, 13(1-2), 24-30.

Bounds, C.O., Upadhyay, J., Totaro, N., Thakuri, S., Garber, L., Vincent, M., Huang, Z., Hupert, M., Pojman, J.A. 2013. Fabrication and Characterization of Stable Hydrophilic 74 Microfluidic Devices Prepared via the in Situ Tertiary-Amine Catalyzed Michael Addition of Multifunctional Thiols to Multifunctional Acrylates. ACS applied materials & interfaces, 5(5), 1643-1655.

Burge, R., Dawson-Hughes, B., Solomon, D.H., Wong, J.B., King, A., Tosteson, A. 2007. Incidence and Economic Burden of Osteoporosis-Related Fractures in the United States, 2005–2025. Journal of Bone and Mineral Research, 22(3), 465-475.

Degasne, I., Basle, M.F., Demais, V., Hure, G., Lesourd, M., Grolleau, B., Mercier, L., Chappard, D. 1999. Effects of roughness, fibronectin and vitronectin on attachment, spreading, and proliferation of human osteoblast-like cells (Saos-2) on titanium surfaces. Calcif Tissue Int, 64(6), 499-507.

Di Maggio, N., Piccinini, E., Jaworski, M., Trumpp, A., Wendt, D.J., Martin, I. 2011. Toward modeling the bone marrow niche using scaffold-based 3D culture systems. Biomaterials, 32(2), 321-9.

Gaalen, S.v., Kruyt, M., Meijer, G., Mistry, A., Mikos, A., Beucken, J.v.d., Jansen, J., Groot, K.d., Cancedda, R., Olivo, C., Yaszemski, M., Dhert, W. 2008. Chapter 19 - Tissue engineering of bone. in: Tissue Engineering, (Eds.) B. Clemens van, T. Peter, L. Anders, H. Jeffrey, F.W. David, C. Ranieri, D.d.B. Joost, P.T.A.L.J.H.D.F.W.R.C.J.D.d.B. Jérôme SohierA2 - Clemens van Blitterswijk, S. Jérôme, Academic Press. Burlington, pp. 559-610.

Garber, L., Chen, C., Kilchrist, K.V., Bounds, C., Pojman, J.A., Hayes, D. 2013. Thiol-acrylate nanocomposite foams for critical size bone defect repair: A novel biomaterial. Journal of Biomedical Materials Research Part A, 10(12), 3531-3541.

Gertzman, A.A., Sunwoo, M.H. 2000. Malleable paste for filling bone defects, Google Patents.

He, J., Genetos, D.C., Leach, J.K. 2010. Osteogenesis and trophic factor secretion are influenced by the composition of hydroxyapatite/poly(lactide-co-glycolide) composite scaffolds. Tissue Eng Part A, 16(1), 127-37.

Ho, S.T., Hutmacher, D.W. 2006. A comparison of micro CT with other techniques used in the characterization of scaffolds. Biomaterials, 27(8), 1362-1376. 75

Hutmacher, D.W. 2000. Scaffolds in tissue engineering bone and cartilage. Biomaterials, 21(24), 2529-2543.

Karageorgiou, V., Kaplan, D. 2005. Porosity of 3D biomaterial scaffolds and osteogenesis. Biomaterials, 26(27), 5474-91.

Lawrence, B.J., Madihally, S.V. 2008. Cell colonization in degradable 3D porous matrices. Cell Adhesion & Migration, 2(1), 9-16.

Levine, B. 2008. A New Era in Porous Metals: Applications in Orthopaedics. Advanced Engineering Materials, 10(9), 788-792.

Liu, Q., Cen, L., Yin, S., Chen, L., Liu, G., Chang, J., Cui, L. 2008a. A comparative study of proliferation and osteogenic differentiation of adipose-derived stem cells on akermanite and β-TCP ceramics. Biomaterials, 29(36), 4792-4799.

Liu, Q., Cen, L., Yin, S., Chen, L., Liu, G., Chang, J., Cui, L. 2008b. A comparative study of proliferation and osteogenic differentiation of adipose-derived stem cells on akermanite and β-TCP ceramics. Biomaterials, 29(36), 4792-4799.

Livak, K.J., Schmittgen, T.D. 2001. Analysis of relative gene expression data using real-time quantitative PCR and the 2(-Delta Delta C(T)) Method. Methods, 25(4), 402-8.

Lopez, M.J., McIntosh, K.R., Spencer, N.D., Borneman, J.N., Horswell, R., Anderson, P., Yu,

G., Gaschen, L., Gimble, J.M. 2009. Acceleration of spinal fusion using syngeneic and allogeneic adult adipose derived stem cells in a rat model. Journal of Orthopaedic Research, 27(3), 366-373.

Mehrkens, A., Muller, A.M., Schafer, D., Jakob, M., Martin, I., Scherberich, A. 2009. Towards an intraoperative engineering of osteogenic grafts from the stromal vascular fraction of human adipose tissue. Swiss Medical Weekly, 139(23-24), 23S-23S.

Milat, F., Ng, K.W. 2009. Is Wnt signalling the final common pathway leading to bone formation? Molecular and cellular endocrinology, 310(1-2), 52-62.
Otsu, N. 1975. A threshold selection method from gray-level histograms. Automatica, 11(285- 296), 23-27.

Pallua, N., Suscheck, C.V. 2010a. Tissue engineering: from lab to clinic. Springer Verlag.

Pallua, N., Suscheck, C.V. 2010b. Tissue Enginnering: from lab to clinic. Springer Verlag.

Papadimitropoulos, A., Scherberich, A., Guven, S., Theilgaard, N., Crooijmans, H.J., Santini, F., Scheffler, K., Zallone, A., Martin, I. 2011. A 3D in vitro bone organ model using human progenitor cells. Eur Cell Mater, 21, 445-58.

Qureshi, A.T., Monroe, W.T., Dasa, V., Gimble, J.M., Hayes, D.J. 2013. miR-148b–Nanoparticle conjugates for light mediated osteogenesis of human adipose stromal/stem cells. Biomaterials, 34(31), 7799-7810.

Qureshi, A.T., Terrell, L., Monroe, W.T., Dasa, V., Janes, M.E., Gimble, J.M., Hayes, D.J. 2012. Antimicrobial biocompatible bioscaffolds for orthopaedic implants. Journal of Tissue Engineering and Regenerative Medicine, n/a-n/a.

Reynaud, E., Jouen, T., Gauthier, C., Vigier, G., Varlet, J. 2001. Nanofillers in polymeric matrix: a study on silica reinforced PA6. Polymer, 42(21), 8759-8768.

Rydholm, A.E., Held, N.L., Benoit, D.S.W., Bowman, C.N., Anseth, K.S. 2008. Modifying network chemistry in thiol-acrylate photopolymers through postpolymerization functionalization to control cell-material interactions. Journal of Biomedical Materials Research Part A, 86A(1), 23-30.

Rydholm, A.E., Reddy, S.K., Anseth, K.S., Bowman, C.N. 2006. Controlling network structure in degradable thiol-acrylate biomaterials to tune mass loss behavior. Biomacromolecules, 7(10), 2827-2836.

Scherberich, A., Galli, R., Jaquiery, C., Farhadi, J., Martin, I. 2007. Three-dimensional perfusion culture of human adipose tissue-derived endothelial and osteoblastic progenitors generates osteogenic constructs with intrinsic vascularization capacity. Stem cells, 25(7), 1823-9.

Schulte, F.A., Ruffoni, D., Lambers, F.M., Christen, D., Webster, D.J., Kuhn, G., Müller, R. 2013. Local Mechanical Stimuli Regulate Bone Formation and Resorption in Mice at the Tissue Level. PloS one, 8(4), e62172.

Singh, R., Lee, P.D., Lindley, T.C., Dashwood, R.J., Ferrie, E., Imwinkelried, T. 2009. Characterization of the structure and permeability of titanium foams for spinal fusion devices. Acta Biomater, 5(1), 477-87.

Sundelacruz, S., Kaplan, D.L. 2009. Stem cell-and scaffold-based tissue engineering approaches to osteochondral regenerative medicine. Seminars in cell & developmental biology. Elsevier. pp. 646-655.

Topart, P., Vandenbroucke, F., Lozac'h, P. 2005. Tisseel versus tack staples as mesh fixation in totally extraperitoneal laparoscopic repair of groin hernias. Surgical Endoscopy And Other Interventional Techniques, 19(5), 724-727.

Yeh, J.C., Tucker, N. 2005. The Use of Tisseel in Oculoplastics. Invest. Ophthalmol. Vis. Sci., 46(5), 4252.

Zanetti, A.S., McCandless, G.T., Chan, J.Y., Gimble, J.M., Hayes, D.J. 2012. Characterization of novel akermanite:poly-ε-caprolactone scaffolds for human adipose-derived stem cells bone tissue engineering. Journal of Tissue Engineering and Regenerative Medicine, n/an/a.

Zanetti, A.S., Sabliov, C., Gimble, J.M., Hayes, D.J. 2013. Human adipose-derived stem cells and three-dimensional scaffold constructs: A review of the biomaterials and models currently used for bone regeneration. Journal of Biomedical Materials Research Part B: Applied Biomaterials, 101(1), 187-199.

Zhang, R., Ma, P.X. 1999. Poly(alpha-hydroxyl acids)/hydroxyapatite porous composites for bone-tissue engineering. I. Preparation and morphology. J Biomed Mater Res, 44(4), 446-55.

CHAPTER 3 SUMMARY AND FUTURE WORK

The work described above was published in *Tissue Engineering Part A.* I was a coauthor on this publication (Chen, C., Garber, L., **Smoak, M.**, and D. Hayes, 2015). The step growth nature of the amine catalyzed Michael addition reaction alleviated the concern of unreacted monomer or radicals leaching into the body as would typically occur using a chain-growth mechanism involving a free-radical process. *In situ* polymerization opens the opportunity for the development of absorbable foams for the conformal repair of critical sized tissue defects, which can be easily delivered in the clinical surgical setting. This represents a substantial improvement over PCL, which are foamed externally prior to surgical insertion, and methylmethacrylate bone cements, which are largely inert, non-porous, and permanent. The SEM analysis, mechanical testing, and micro CT data prove that there is no distinct difference between the PETA-co-TMPTMP foam made in situ and in vitro. While this material has many advantages, future work includes the development of a homogenous HA containing polymer network, osteogenic studies and improved mechanical strength of the foamed PETA-co-TMPTMP with varying HA amounts. It is clear that scaffold technology plays a critical role in the success of the current stem cell based bone tissue engineering paradigms. While a variety of different materials, both ceramics and polymers have been tested in combination with hASCs, Lendeckel et al. and others note that composite scaffolds may offer a better clinical outcome as a result of improved mechanical and biological properties.(Lendeckel et al., 2004) Calcium phosphate nanoscale ceramic particles of HA and β-TCP will be used as the inorganic osteogenic phase and thixotropic agent in future studies.

By gas foaming thiol-acrylate based copolymers synthesized via Michael addition with an in situ amine-catalyst, a porous polymeric scaffold with bone-like morphology was developed

as a potential graft or augment in critical-sized bone defect repair. Not only does PETA:HA composite have substantial porosity and interconnectivity, it also demonstrates adequate mechanical strength as compared to cortical bone. Compared to PCL:HA composites, both PETA:HA (85:15) and PETA:HA (80:20) scaffolds showed higher mineral deposition and ALP and OCN expression level. Overall, the PETA:HA had higher compressive strength and improved cytocompatibility compared to PCL controls. Mesenchymal cells cultured on PETA based scaffolds had a greater expression of osteogenic markers and the scaffolds exhibited significantly greater mineralization than hASC cultured on PCL controls. The *in vivo* study demonstrated that animals injected with PETA:HA composites showed no signs of surgical site or systemic toxicity and that PETA:HA composites induced osteogenesis in vivo. Additionally, the study serves as a proof-of-concept that gas foaming of thiol-acrylate polymers *in vivo* may be used to conformally fill irregular sized defects.

In addition, silver nanoparticles were able to be incorporated into this polymer to inhibit the proliferation of gram positive and gram negative bacteria. Silver nanoparticles are natural anti-bacterial agents. Through a coating method, the silver nanoparticles leached into the physiological solution (PBS) and inhibited the growth of *Staphylococcus aureus* (99.5%) and E*scherichia coli* by (99.9%), bacteria often associated with surgical site infections (Smoak, et al., 2014). In addition, I sought to overcome the limitations of this polymer as part of my senior design project to build a better composite for bone tissue engineering.